20th AIAA Computational Fluid Dynamics Conference
27 - 30 June 2011, Honolulu, Hawaii

AIAA 2011-3536

An Evolutionary Geometry Parametrization for Aerodynamic Shape Optimization

Xiaocong Han* and David W. Zingg†
Institute for Aerospace Studies, University of Toronto
4925 Dufferin St., Toronto, Ontario, M3H 5T6, Canada

An evolutionary geometry parametrization is presented for aerodynamic shape optimization. The geometry parametrization technique is constructed by integrating the traditional B-spline approach with a knot insertion procedure. It is capable of defining a sequence of nested parametrizations with the number of design variables being gradually enlarged. The optimization coupled with this technique is carried out sequentially from the basic parametrization to more refined parametrizations, as long as the geometry can be continuously improved. Due to the nature of the B-spline formulation, feasible parametrization refinements are not unique. Guidelines based on sensitivity analysis and geometric constraints are developed to assist the automation. The proposed process is applied to several optimization examples to demonstrate its effectiveness.

I. Introduction

Motivated by the need to reduce jet fuel consumption and greenhouse gas emissions, there is an increase in demand for efficient aircraft with possibly novel, unconventional aerodynamic configurations. Based on improvements in computational fluid dynamics (CFD) and high performance computing capabilities, numerical aerodynamic shape optimization has become a promising component in the development of such aircraft and has been widely adopted in aerospace industry. However, with the increasing complexity of design problems, shape optimization for aerodynamic applications remains a costly task and further improvements in efficiency are needed.

One well recognized problem in aerodynamic shape optimization is attributed to an excessive number of design variables. A number of authors[1–3] have pointed out that the presence of a large number of design variables results in poor performance for most existing optimization algorithms. Thus, it is essential to include a limited number of critical design variables in an optimization, and the challenge of choosing design variables is faced by a designer. However, prescribing design variables is not an ideal treatment for an automated optimization process, especially when an unconventional configuration is subjected to some unfamiliar design objectives; human intervention could mislead the optimization and should be minimized. Consequently, it is desirable to organize a problem as a succession of optimizations with an increasing number of significant design variables, and these variables should be deduced based on the performance of the existing geometry.

In order to build such a process, it is critical to have a flexible and consistent definition for design variables. For aerodynamic shape optimization problems, this specifically refers to a geometry representation technique that is able to continuously refine the parametrization and produce a gradually enlarged set of design variables. We regard such a technique as an evolutionary geometry parametrization, and it requires two essential conditions:

- Multiple parametrization refinements can be carried out in a consistent manner;
- The geometry should not be changed as its parametrization is refined.

*Graduate Student
†Professor, Tier I Canada Research Chair in Computational Aerodynamics, J. Armand Bombardier Foundation Chair in Aerospace Flight, Associate Fellow AIAA

There exist a large variety of parametrization methods for various applications.[4–6] However, some techniques like extended Joukowski transformation[7] and PARSEC[8] require predetermined design variables, so they are not suitable to form the proposed parametrization. Other commonly used approaches, such as discrete grid points,[9] domain elements,[10] basis shape functions,[11,12] and polynomial splines[13] possess enough flexibility and can be considered for modification into an evolutionary parametrization.

Attempts of performing optimization with a changing parametrization have been carried out by several authors. Beux and Dervieux[1] describe a gradient-based multilevel optimization using surface grid point coordinates as design variables. They defined a hierarchical parametrization by extracting different subsets of grid points from the complete surface points forming a family of embedded levels (i.e. a coarse level corresponds to a small number of grid points, and a fine level refers to a large number of grid points). With this nested parametrization, they proposed two optimization sequences: first, the optimizations are conducted sequentially from the coarsest level to the finest level; second, multigrid strategies are adopted. The optimizations are performed at the various levels according to a full V-cycle sequence. Their results display an increase of optimization efficiency due to this process.

Similar research has also been accomplished by Desideri and colleagues.[2,14,15] Their parametrization strategy is defined by Bezier curves and volumes with a degree elevation algorithm. In these works optimizations are carried out on different parametrizations following a prescribed sequence. They have implemented both gradient-based and gradient-free optimizers, and considerable improvements are achieved.

In this paper, evolutionary geometry parametrization is constructed based on an existing B-spline curve formulation for airfoils[16] and a B-spline volume parametrization for general three-dimensional geometries and associated volume grids.[17] This process consists of a B-spline approximation and a series of knot insertions. The difference between this approach and the above methods is that the knot insertion procedure is not unique due to the intrinsic properties of B-spline formulation. Therefore, parametrization refinements cannot be predetermined but can be selected during the optimization process. As a result, the proposed optimization is carried out sequentially from the initial parametrization to more refined parametrizations as long as the objective function continues to improve.

The rest of the paper is constructed as follows: Section II describes the B-spline formulations; Section III briefly reviews the mesh movement algorithm, the flow solver and the optimizer used in the optimization problems; Section IV explains the optimization procedure associated with an evolutionary parametrization; sSection V presents the results of optimization problems; finally, Section VI concludes the paper and indicates areas for future work.

II. B-spline parametrization

A B-spline method uses the tensor product of polynomial basis functions and corresponding coefficient vectors to analytically represent a shape. Because the basis functions are predefined in the parametric domain, the locations of the coefficient vectors, known as control points, determine the shape. Hence these control points are naturally chosen as design variables for an optimization. An evolutionary parametrization based on B-spline formulation has two stages. First, a basic parametrization consisting of the initial set of control points is generated; second, refined parametrizations with more control points are constructed using the knot insertion algorithm. The details of this procedure are presented using an airfoil and a rectangular wing as examples.

II.A. B-spline curve

A planar B-spline curve is used to describe the surface of an airfoil. It is defined as a mapping from the one-dimensional parametric space $\{\xi \in \mathbb{R}\}$ to the two-dimensional physical space $\left\{\mathbf{X}_a \in \mathbb{R}^2\right\}$ of the following form:

$$\mathbf{X}(\xi) = \sum_{i=1}^{n} \mathbf{d}_i \, \mathcal{N}_{i,k}(\xi) \tag{1}$$

$\mathbf{X}(\xi)$ is the B-spline curve. With a given airfoil, the purpose of this procedure is to produce a B-spline curve that best approximates its surface; ξ is the parameter that is generated by mapping each surface point on the airfoil to a parametric space; the coefficient vectors, $\{\mathbf{d}_i : i = 1, \ldots, n\}$, are the n control points; the functions, $\{\mathcal{N}_{i,k} : i = 1, \ldots, n\}$, are the normalized polynomial basis functions of order k.

A few essential choices will significantly affect the quality of an approximation. The choice of the mapping parameter is one of them. As denoted in the work of Kulfan,[18] for an airfoil with a round nose, the following centripetal parametrization[19] gives desirable results.

$$\xi_1 = 0 \tag{2}$$

$$\xi_j = \frac{n-k-1}{L_T} \sum_{m=1}^{j-1} \sqrt{L_m} \qquad j = 2, \ldots, N \tag{3}$$

Here N is the total number of surface points on the airfoil, L_m is the segment length between successive points, and the normalization factor, L_T is given by

$$L_T = \sum_{m=1}^{N-1} \sqrt{L_m} \tag{4}$$

The above mapping defines a parametric domain, $\xi \in [0, n-k-1]$. Another concept associated with this mapping is a knot vector that partitions the parametric domain. This partition determines the distribution of the basis functions, which has an important impact on the parametrization. Many authors[20,21] have experimented with different choices. The cosine function adopted here turns out be a good compromise between robustness and accuracy:

$$t_i = \begin{cases} 0 & 1 \le i \le k \\ \frac{n-k-1}{2}\left[1 - \cos\left(\frac{i-k}{n-k-1}\,\pi\right)\right] & k+1 \le i \le \frac{n+k-3}{2} \\ \frac{n-k-1}{2} & \frac{n+k-1}{2} \le i \le \frac{n+k+3}{2} \\ \frac{n-k-1}{2}\left[1 - \cos\left(\frac{i-k-2}{n-k-1}\,\pi\right)\right] & \frac{n+k+5}{2} \le i \le n \\ n-k-1 & n+1 \le i \le n+k \end{cases} \tag{5}$$

Note the multiple knots appearing at the middle and two ends of the knot vector; they ensure one control point is placed at the leading edge of the airfoil and two control points coincide at the trailing edge of the airfoil. Because the multiplicity of a knot decreases the continuity of the associated curve, the repeated knots at two ends will generate a desirable sharp trailing edge, but the continuity reduction at the leading edge is unwanted. To overcome this problem, two adjacent control points are placed colinearly with the leading edge point, so that C^1 continuity is restored. This amendment is performed at the end of the approximation.

Once the parametric domain is fully defined, the basis functions can be deduced by a recursive relation[22] of the following form:

$$\mathcal{N}_{i,1}(\xi) = \begin{cases} 1 & \text{if } \ t_i \le \xi \le t_{i+1} \\ 0 & \text{otherwise} \end{cases} \tag{6}$$

$$\mathcal{N}_{i,k}(\xi) = \frac{\xi - t_i}{t_{i+k-1} - t_i}\, \mathcal{N}_{i,k-1}(\xi) + \frac{t_{i+k} - \xi}{t_{i+k} - t_{i+1}}\, \mathcal{N}_{i+1,k-1}(\xi) \tag{7}$$

Based on Eq. 1, in order to determine the B-spline curve, locations of control points must be provided. Assume the airfoil surface is defined by a set of points, $\{\mathbf{P}_j, j = 1, \ldots, N\}$. The control points can be determined by solving the least squares problem, min $\sum_{j=1}^{N} ||\mathbf{P}_j - \mathbf{X}_j||_2$. This process can be further improved using an iterative parameter correction algorithm proposed by Hoschek,[23] which optimizes the mapping parameter for each surface point.

One example of an approximation using a 4th-order B-spline curve is shown in Figure 1(a). The NACA0012 airfoil is described using 15 control points, and the leading edge is handled by keeping three adjacent control points aligned and equidistant.

II.B. Knot insertion

Adding control points to the existing B-spline curve is accomplished through knot insertion. Boehm[24] demonstrated that a new knot can be added into the existing knot vector without changing the shape of

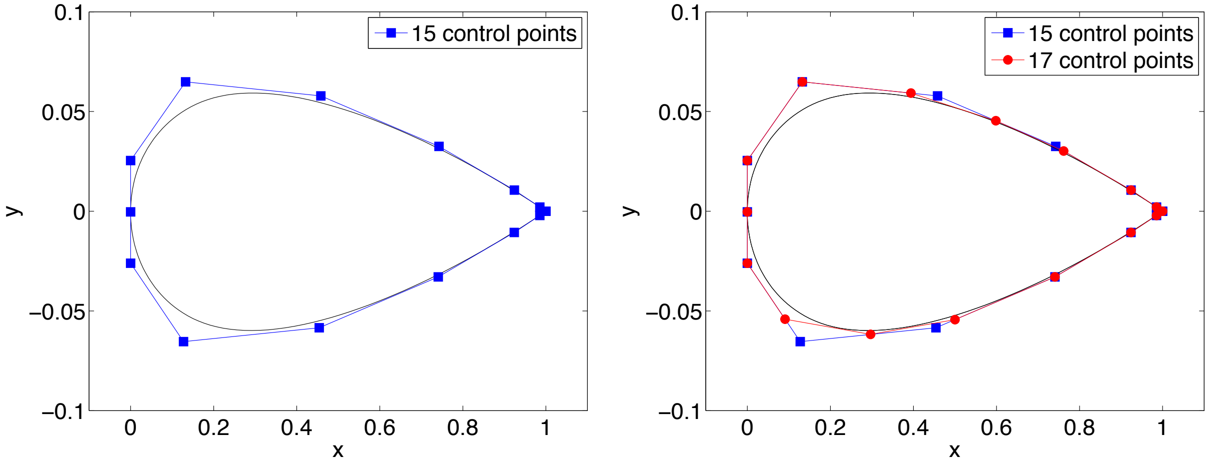

(a) initial parametrization (b) refined parametrization

Figure 1. B-spline parameterization of the NACA0012 airfoil. Plot (a) depicts the parametrized surface and control points; plot (b) shows the refined parametrization with the additional control points.

the B-spline curve. Thus the geometry is preserved regardless the increased of the number of control points. However, if the new knot to be inserted already exists in the knot vector, then adding a repeated knot would result in a decrease in continuity. Therefore, inserting repeated knots is avoided.

Inserting a new knot obeys the following procedure. Denoting the new set of control points with a superscript $*$, if a knot t^* is added to (t_r, t_{r+1}), the new control points $\{\mathbf{d}_i^* : i = 1, \ldots, r-k+1, r+1, \ldots, n+1\}$ retain the positions of the old control points based on the local support property of the B-spline formulation:

$$\mathbf{d}_i^* = \mathbf{d}_i \qquad 1 \leq i \leq r-k+1 \tag{8}$$

$$\mathbf{d}_i^* = \mathbf{d}_{i-1} \qquad r+1 \leq i \leq n+1 \tag{9}$$

The new control points, $\{\mathbf{d}_i^* : i = r-k+2, \ldots, r\}$, are placed on the control polygon formed by the old control points, $\{\mathbf{d}_i^* : i = r-k+1, \ldots, r\}$. The quantitative relation can be deduced using the de Boor algorithm:[22]

$$\mathbf{d}_i^* = (1-\alpha_i)\,\mathbf{d}_{i-1} + \alpha_i\,\mathbf{d}_i \tag{10}$$

$$\alpha_i = \frac{t^* - t_i}{t_{i+k-1} - t_i} \tag{11}$$

The above procedure creates new control points located on the old control polygon, but their exact coordinates are unknown in advance. If a user specified control point $\mathbf{d}^*$ between $(\mathbf{d}_r, \mathbf{d}_{r+1})$ is required, this procedure can be reversed to calculate the required knot:[25]

$$s = \frac{\mathbf{d}^* - \mathbf{d}_r}{\mathbf{d}_{r+1} - \mathbf{d}_r} \tag{12}$$

$$t^* = t_{r+1} + s(t_{r+k} - t_{r+1}) \tag{13}$$

Figure 1(b) uses the parametrized NACA0012 airfoil as an example. One knot insertion takes place at the interval (t_{13}, t_{14}) on the upper surface, splitting this knot interval into two parts that contain approximately same number of parameters. This insertion strategy is adopted in all examples presented, unless otherwise stated. Another inverse knot insertion occurs on the lower surface, generating a new control point located at $x = 0.5$. In both cases, the geometry is precisely maintained.

II.C. B-spline volume

The B-spline volume parametrization developed by Hicken and Zingg[17] is employed in the three-dimensional shape optimization problems. Instead of only parametrizing the surface of the object, this approach represent the entire computational grid with a B-spline volume control mesh. Thus, the shape deformation is acquired through the movement of the B-spline surface patches, and the corresponding grid perturbation is driven by the adjustment of the B-spline volume control mesh to conform to the surface changes. The B-spline volume method is formulated by extending planar B-spline curves into multi-dimensional space. This defines a mapping from a parametric space, $\{\boldsymbol{\xi} = (\xi, \eta, \zeta) \in \mathbb{R}^3 : (\xi, \eta, \zeta) \in [0, 1]\}$ to the physical space $\{\mathbf{X}(\boldsymbol{\xi}) \in \mathbb{R}^3\}$. The tensor product representation is given by

$$\mathbf{X}(\boldsymbol{\xi}) = \sum_{i=1}^{n_i} \sum_{j=1}^{n_j} \sum_{k=1}^{n_k} \mathbf{d}_{ijk}\, \mathcal{N}_{i,p_i}(\xi)\, \mathcal{N}_{j,p_j}(\eta)\, \mathcal{N}_{k,p_k}(\zeta) \tag{14}$$

Here, the B-spline volume, $\mathbf{X}(\boldsymbol{\xi})$, and the control points, $\mathbf{d}_{ijk}$'s, have analogous characteristics to the B-spline curve and control points. However, the mapping parameter, $\boldsymbol{\xi}$ is defined using a traditional chord length parametrization for the purpose of approximating structured multi-block grids. The basis functions are defined separately for each parameter. Theoretically, the orders of the basis functions are independent for different parameters, but in practical applications, the order of polynomial basis functions is usually set to be the same for each parameter to maintain the same continuity condition. Hence, the order of the basis functions is denoted by p for the rest of the work. The computation of the basis functions still refers to the recursive definition but with spatially varying knot vectors. Taking basis functions in the ξ direction as an example, they are given by

$$\mathcal{N}_{i,1}(\xi) = \begin{cases} 1 & t_i(\eta,\zeta) \le \xi \le t_{i+1}(\eta,\zeta) \\ 0 & \text{otherwise} \end{cases} \tag{15}$$

$$\begin{aligned} \mathcal{N}_{i,p}(\xi) = & \left(\frac{\xi - t_i(\eta,\zeta)}{t_{i+p-1}(\eta,\zeta) - t_i(\eta,\zeta)} \right) \mathcal{N}_{i,p-1}(\xi) \\ & + \left(\frac{t_{i+p}(\eta,\zeta) - \xi}{t_{i+p}(\eta,\zeta) - t_{i+1}(\eta,\zeta)} \right) \mathcal{N}_{i+1,p-1}(\xi) \end{aligned} \tag{16}$$

where the knot vector, $t_i(\eta,\zeta)$, is a spatially varying function of parameters, η and ζ. Its form can be arbitrarily set to accommodate the different geometries, as long as it remains non-decreasing. For the grids made of hexahedra, a simple bilinear form is used.[17]

$$t(\eta,\zeta) = t(0,0)(1-\eta)(1-\zeta) + t(1,0)\eta(1-\zeta) + t(0,1)(1-\eta)\zeta + t(1,1)\eta\zeta \tag{17}$$

Here $t(0,0)$, $t(1,0)$, $t(0,1)$ and $t(1,1)$ are four edge knot vectors in the ξ direction, and they are constructed to have roughly the same number of parameters in each knot interval.

The B-spline volume control points are determined by solving Eq. 14 through a least squares procedure. For multi-block grids, consistent positions of control points at interfaces are mandatory. Thus the least squares problem is solved sequentially for block edges, surfaces, and volumes. The resulting B-spline volume control points are also referred as a volume control mesh. Figure 2(a) shows the control mesh of a rectangular wing with 7 control points in the spanwise and streamwise directions using 4th-order basis functions and bilinear spatially varying knot vectors.

Creating a refined control mesh for an existing B-spline volume can also be achieved using a knot insertion algorithm. From Eq. 17, one can observe that the edge knot vectors are spatially invariant; this implies that the knot insertion algorithm for B-spline curves is still applicable to these edge knot vectors. Since the grids used in this work consist of hexahedra, once the four edge knot vectors in the same direction are refined simultaneously, all the other knot vectors in this direction can be subsequently refined using Eq. 17. Hence, by re-solving the least squares problem, a new B-spline volume can be established with a refined control mesh. Referring to the local support property of the B-spline formulation, only some of the control points will be altered on the edges, which implies that the change to the control mesh will be limited to the corresponding sections. Figure 2(b) illustrates a control mesh refinement in the spanwise direction (one more section is added).

III. Overview of optimization routines

In order to perform an automated aerodynamic shape optimization, a set of analysis and optimization routines are integrated together. The present optimization codes in two and three dimensions contain the

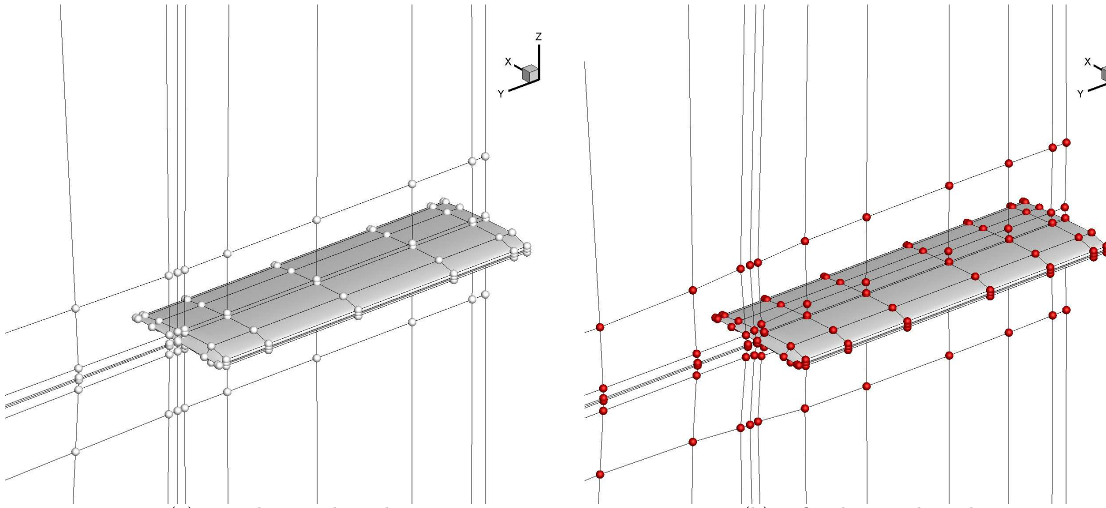

(a) initial control mesh (b) refined control mesh

Figure 2. B-spline parameterization of a rectangular wing. The white spheres in plot (a) are the original control points and the red spheres in plot (b) are the refined control points.

following essential components: 1) geometry parametrization, 2) grid movement algorithm, 3) flow solver, 4) optimizer. Among them, the geometry parametrization using B-spline formulation is described in detail in the previous section. A brief overview of the remaining routines is given here.

During the optimization, once the geometry is modified by manipulation of the surface control points, the computational grid has to conform to the new shape. Nemec et al.[26] proposed an algebraic grid movement algorithm that preserves the location of the outer grid boundary and relocates the grid points in the normal direction proportional to the distance from the surface. This approach is demonstrated to be robust and efficient for small shape changes. Truong et al.[27] implemented a mesh movement algorithm based on the linear elasticity equations with multiple increments. This method is able to accommodate relatively large shape variation occurred in the optimization, but is also computationally expensive. Hicken and Zingg[17] integrated the linear elasticity grid movement algorithm with the B-spline volume formulation such that the relatively coarse control mesh is moved by the algorithm, and the fine computational grid is regenerated using the perturbed control mesh. Because usually there are two to three orders of magnitude fewer control points than grid points, this approach is very efficient. In the present work, the algebraic grid movement is used in the two-dimensional airfoil optimizations and the linear elasticity grid movement of the control mesh is adopted in three-dimensional wing optimizations.

To evaluate the aerodynamic performance of an existing geometry, a high fidelity flow solver is necessary. For a two-dimensional airfoil, an efficient Newton-Krylov flower solver was developed by Nemec and Zingg[16] solving the Reynolds-averaged Navier-Stokes equations with the Spalart-Allmaras turbulence model. Spatial derivatives in the governing equations are discretized by the second-order centered difference scheme, and temporal derivatives are neglected for steady solution. The resulting flow residual equations are solved using a Newton-Krylov strategy. The implicit Euler time marching method with approximate-factorization is used to provide an initial value for the Newton iterations, and the generalized minimal residual method is adopted to solver the linear systems. In the three-dimensional optimization code, a parallel Newton-Krylov-Schur Euler solver developed by Hicken and Zingg[28] is used. This solver adopts a similar Newton-Krylov strategy, but for the results presented in this paper, the start-up algorithm is changed to the dissipation-based homotopy continuation,[29] and the linear solver is changed to the flexible GMRES with an approximate-Schur preconditioner.

The SNOPT computational package[30] is used as the optimizer. This algorithm handles constraints by forming a modified Lagrangian and searches local optimal points that satisfy the KKT optimality conditions. It adopts a sequential quadratic programming method; each quadratic subproblem is created based on the approximated Hessian of the Lagrangian using a BFGS method. Since SNOPT is a gradient-based algorithm, the gradients of objective functions and constraints are evaluated using the well established discrete adjoint method.[17,26,31] In the present code for airfoil optimization, the grid sensitivities are treated implicitly; in three dimensions, the grid sensitivities are handled through mesh adjoint equations.

IV. Optimization procedure

Having all the numerical routines available, an automated optimization process can be established with the aid of an evolutionary B-spline parametrization. Since this evolutionary parametrization is able to produce consistent geometry representations as the number of control point gradually increases, the proposed process is executed in a progressive manner: initially, an optimization is started with relatively few control points; once it converges or is close to convergence, the geometry parametrization is refined, and the next optimization begins with more control points based on the obtained geometry. This procedure repeats continuously until the final termination. To clearly present the results, finding an optimized geometry is regarded to be a completion of an optimization cycle.

The knot insertion algorithm can be performed at different knot intervals, so the additional control points can be placed at various locations. To choose the most effective control points among all the candidates, we have established the following selection criteria:

1. The number of parameters in the each knot interval should remain above a certain threshold. Since the B-spline control points are locally supported, clustering excessive control points in some region would not lead to significant improvement.

2. Local non-linear constraints such as minimum thickness, critically impact the movement of control points. If a constraint is inactive, it implies that there exists a feasible region in the design space, and adding control points at this location has a large probability to outperform adding control points in a region with active local constraints. Therefore preference is given to refinements which add control points to the regions containing inactive local non-linear constraints.

3. The satisfaction of the linear constraints is mandatory. Any parametrization refinement violating the linear constraints is dropped from consideration.

4. If there are multiple candidates remaining after considering the above requirements, the magnitude of the sensitivity with respect to the proposed new control points is used as a measure of the potential improvement. The prospective control point with the highest sensitivity is selected.

Second, parametrization refinement (i.e. increasing the number of design variables) occurs at regular intervals during the optimization process, but it is hard to identify a clear signal for this procedure. Some authors[1,3] argue that when the number of design variables is small, a small number of optimization iterations is enough and full convergence is unnecessary, since these optimization cycles are only intermediate steps. However others[32,33] point out that the optimizations at the first few cycles should be driven sufficiently close to the optimal shape that the current shape can provide a good start for subsequent optimizations. At the current stage, we choose to perform well converged optimization at each cycle for the following two reasons:

1. It is desirable to have a small number of critical design variables. If a significant improvement is made by existing design variables, the optimization could be terminated without attempting the next cycle. Thus, optimization at each cycle is driven toward convergence to make full use of every design variable.

2. One selection criterion uses the magnitude of the sensitivity as a test of different parametrization refinements. This is only valid if the optimization is fairly well converged.

Moreover, terminating the optimization cycles also requires a criterion. As pointed out in the work of Zingg et al.,[34] the benefit of introducing control points after a certain threshold is marginal. Thus, this process is terminated if significant improvements are not achieved by adding further design variables. Other termination conditions are also posed; they will be stated for each optimization problem.

V. Results

The proposed optimization process based on evolutionary parametrization is applied to aerodynamic shape optimization problems. To demonstrate its effectiveness, the same problems are also solved using varying numbers of control points that are uniformly placed. Here "uniform" means that, for a two-dimensional airfoil, its knot vector obeys the stated cosine function, and for a three-dimensional wing, its knot vectors evenly partition the parametric domain. The results from these two approaches are compared and discussed.

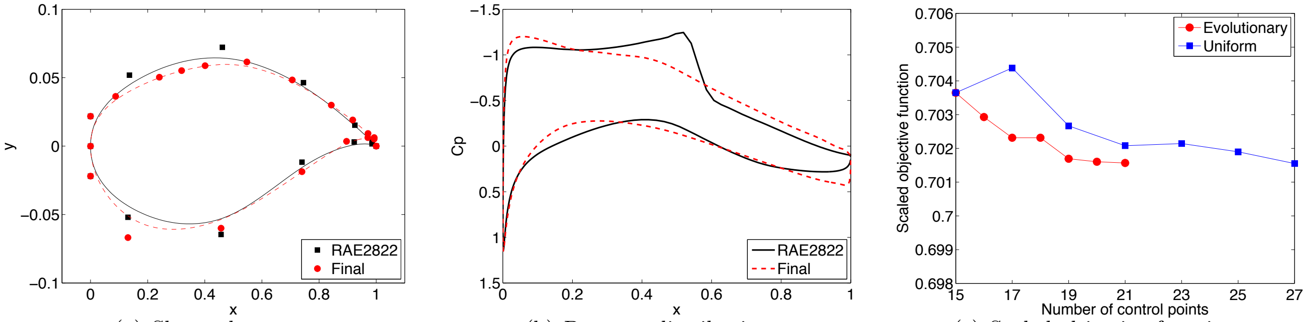

(a) Shape change (b) Pressure distribution (c) Scaled objective function

Figure 3. Lift-constrained drag minimization

Table 1. Geometric constraints for lift constrained drag minimization problem

constraint	1	2	3
location (c)	0.96	0.99	-
minimum thickness (c)	0.006	0.0012	-
minimum area (c^2)	-	-	0.07761

V.A. Airfoil optimization: lift-constrained drag minimization

The objective of this optimization is to minimize the drag coefficient of an airfoil at a Mach number of 0.74 and a Reynolds number of 2.7 million in a fully turbulent flow. The lift coefficient is kept constant at 0.733, and the geometric constraints are listed in Table 1. The initial shape for the optimization is the RAE2822 airfoil. The angle of attack is not treated as a design variable but adjustable to satisfy the lift constraint.[35] The grid has a "C" topology with 289 nodes in the streamwise direction and 65 nodes in the normal direction. We parametrize this initial geometry with 15 B-spline control points evenly placed around the airfoil. Three points at the leading edge and two points at the trailing edge are frozen to prevent translation and unrealistic curvature. The ordinates of the remaining 10 control points serve as design variables.

In this problem, the area constraint affects every design variable, thus it behaves as a global constraint. The thickness constraints only influence the control points close to them, so they are referred to as local constraints. As discussed in Section IV, the parametrization refinement takes into account whether or not these two thickness constraints are active. A geometric restriction is imposed to ensure that each knot interval contains at least 5% of the total mapping parameters (each surface grid point is assigned a parameter by a predetermined mapping strategy, and the parametric domain partition defined by the knot vector requires each knot interval to contain a certain number of parameters so that every control point can control a minimum number of surface grid points), and the entire process is terminated when two successive parametrization refinements result in negligible improvement. Figure 3(a) displays the surface change and the inserted control points upon the completion of the optimization. Figure 3(b) shows a comparison of the pressure distributions. The shock is completely eliminated by the optimized airfoil.

To provide a comparison for optimization efficiency, this result is compared with a series of optimizations with varying numbers of control points uniformly placed around the airfoil. Figure 3(c) depicts such a comparison in terms of the scaled objective function. The scaling factor is the drag coefficient of the original RAE2822 airfoil. This figure shows that the optimization with evolutionary parametrization consistently reduces the drag coefficient in comparison to a uniform placement of design variables. After adding 6 design variables to the original 15 for a total of 21, it is able to reach an optimal solution that is comparable to the result obtained using 27 design variables evenly around the airfoil.

V.B. Airfoil optimization: maximization of lift-to-drag ratio

The second airfoil optimization maximizes the lift-to-drag ratio. The freestream Mach number and Reynolds number are 0.25 and 2.88 million respectively. The seven thickness constraints listed in Table 2 are imposed. The angle of attack is considered a design variable and initially set to 9.0 degrees. The baseline geometry is

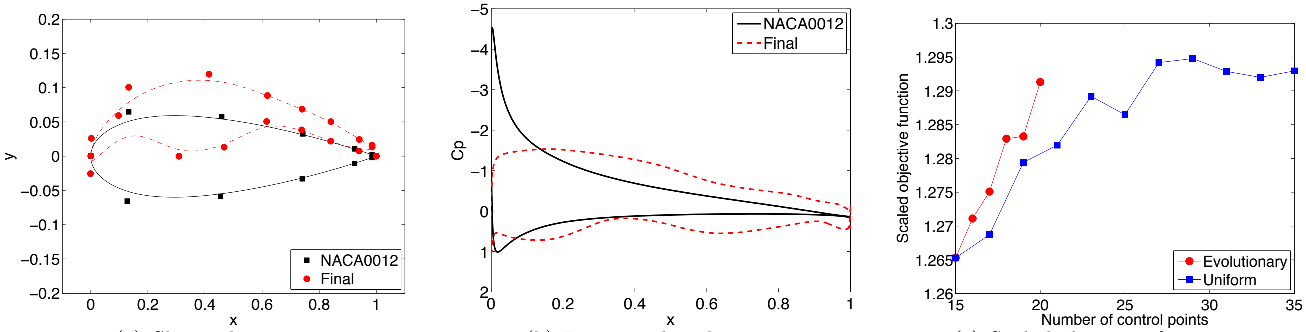

(a) Shape change (b) Pressure distribution (c) Scaled objective function

Figure 4. Lift-to-drag maximization

Table 2. Geometric constraints for lift-to-drag maximization problem

constraint	1	2	3	4	5	6	7
location (c)	0.05	0.35	0.65	0.75	0.85	0.95	0.99
minimum thickness (c)	0.04	0.11	0.04	0.03	0.026	0.012	0.002

the NACA0012 airfoil, and the computational grid has the same size as the previous problem. Initially 15 control points are evenly placed around the airfoil; 10 of them are free to move in the vertical direction.

In this problem, multiple thickness constraints are present. Thus the additional control points are only inserted into the regions where inactive thickness constraints reside, and the optimization sequence is terminated after all the constraints are considered. Figures 4(a) and 4(b) illustrate the change of the geometry and the pressure distribution. The comparison of the evolutionary parametrization and uniform refinements is depicted in Figure 4(c). The objective function value is scaled by the initial lift-to-drag ratio of the NACA0012 airfoil. It can be seen from this figure that the proposed optimization sequence captures more effective design variables. The optimal lift-to-drag ratio is obtained with only 20 control points.

V.C. Planform optimization

The following optimizations are all conducted in a three-dimensional context; the common design objective is to minimize the induced drag at a constrained lift coefficient. Prandtl's lifting line theory[36] concludes that the minimum induced drag for a planar wake occurs when the lift is elliptically distributed. This is considered as a measure for the optimization results.

The B-spline volumes are used to approximate a 12-block flat-plate grid consisting of 1.1 million nodes, and the initial geometry is constructed to be a rectangular wing with a uniform chord of $2/3$, a semi-span of 2, and NACA0012 sections. The chord and span are non-dimensionlized by the chord length of the flat-plate grid. The projected area, $S = 4/3$, is used as the reference area, and remains fixed during the optimization. The freestream Mach number is 0.5, and the lift coefficient is constrained at 0.35. The angle of attack is considered a design variable, and it is initially 3.94321 degrees, which produces the target lift coefficient with the baseline geometry.

The initial parametrization for each block is $7 \times 7 \times 6$. In other words, on the wing surface, there are 7 control points in the streamwise and spanwise directions. To perform an optimization through planform variation, all the control points except the ones on the trailing edge are free to move in the streamwise direction, and the entire trailing edge are fixed to reduce the impact of a nonplanar wake. The leading edge control points possesses complete degrees of freedom, other interior points are coupled with the leading edge control points to provide a scaling once the leading edge changes. Therefore, the initial effective design variables are the 7 chord lengths and the angle of attack. One additional constraint is needed to confine the wing within $-0.5 \leq x \leq 0.5$ with the purpose of maintaining a reasonable shape. The parametrization refinement is formulated such that more spanwise stations are added, so that the effective design variables are gradually increased. By experience, each knot interval is required to maintain at least 15% of the total number of parameters in the spanwise direction, so that the B-spline control points lie sufficiently far apart.

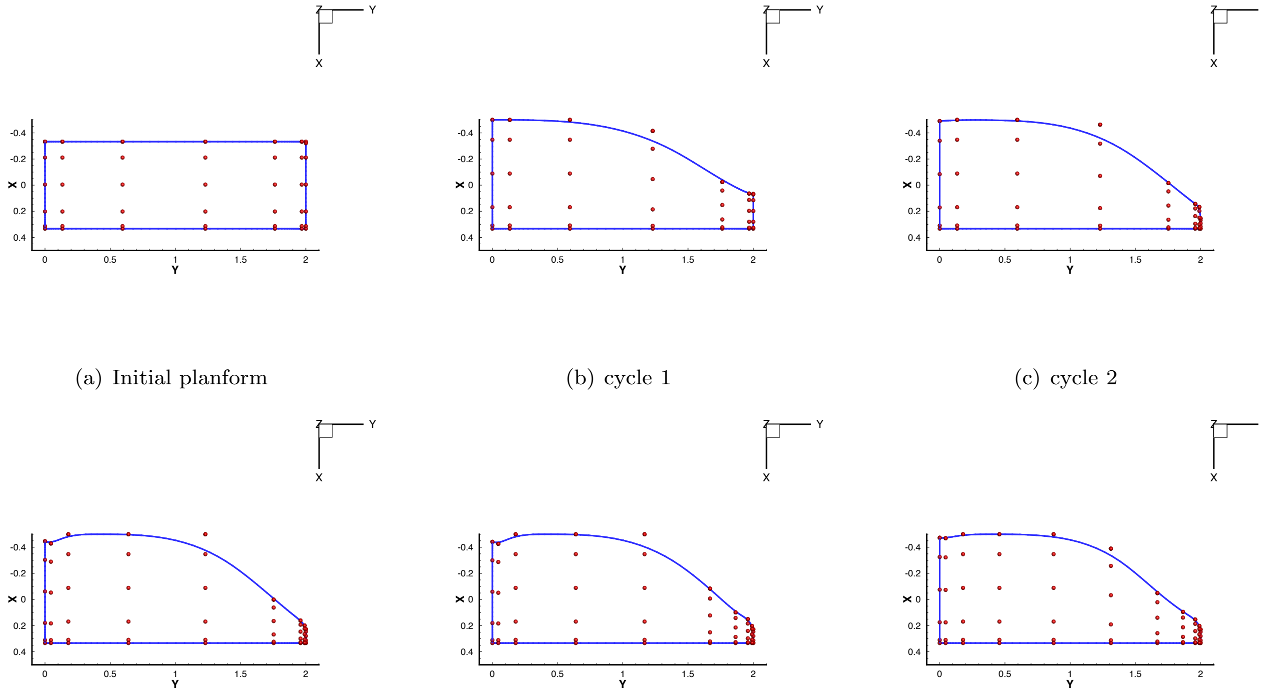

(a) Initial planform (b) cycle 1 (c) cycle 2

(d) cycle 3 (e) cycle 4 (f) cycle 5

Figure 5. Planform changes during the optimization

Figure 5 shows the planform deformation at each optimization cycle. As the more spanwise stations are added, the geometry approaches a crescent shape with decreasing chord lengths along the span. The lift distributions are plotted in Figure 6(a), and it can be seen that the final lift distribution is close to the classical elliptical distribution for the most part but substantially different at the tip. This phenomenon has been identified by Hicken and Zingg,[37] and they point out that the presence of the shape tip causes the vertex to release along the tip edge, which ultimately results in a nonplannar wake. Nevertheless, the purpose of this example is to demonstrate the effectiveness of the evolutionary parametrization. In terms of the performance of the optimized design, the drag coefficient is reduced from 0.006769 to 0.006606; a roughly 2.4% drop is achieved. The span efficiency of the final geometry is 0.9838, which is close to the efficiency of 0.988 obtained by Hicken and Zingg[37] using 15 spanwise control points. Figure 6(b) compares the evolutionary parametrization with uniformly spaced parametrizations. The latter do not receive significant benefits from increasing effective design variables, and their performance is inferior comparing to the evolutionary parametrization using the same number of spanwise control points.

V.D. Winglet optimization

With the purpose of reducing induced drag, the effect of non-planar structure has been well recognized.[38] In this problem, the optimization based on evolutionary parametrization is applied to investigate an optimal spanwise vertical structure that yields minimal induced drag. The baseline geometry is the same rectangular wing used for planform optimization; the operating condition and constraints are also identical to the previous problem. The vertical coordinates of the surface control points are free to move, and a box constraint is imposed to confine the entire geometry within $-0.2 \leq z \leq 0.2$. To prevent excessive degrees of freedom, interior control points at each spanwise station are coupled with the corresponding leading and trailing edges such that the thickness of the section is maintained. Also, to generate reasonable vertical structure, the control points near the wing tip are maintained in a consistent manner. The formed winglet can be either upward or downward with wavy surface details, but an abrupt change of angle is avoided. This is

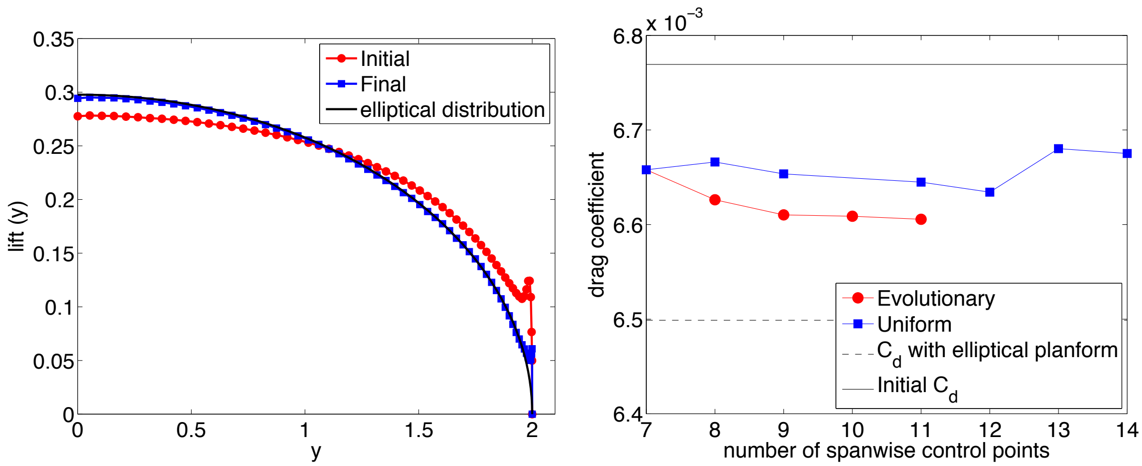

(a) Lift distribution (b) C_D vs. number of sections

Figure 6. Planform optimization

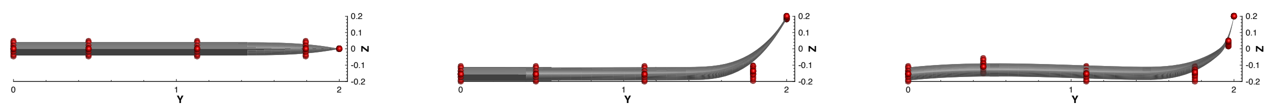

(a) Initial shape (b) cycle 1 (c) cycle 2

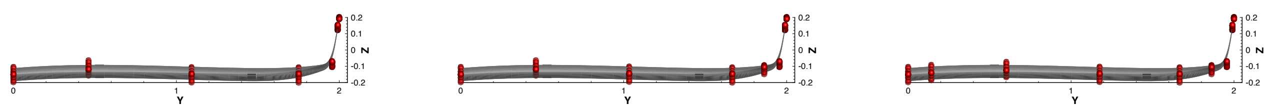

(d) cycle 3 (e) cycle 4 (f) cycle 5

Figure 7. Winglet formation

done by defining the maximum dihedral and anhedral between adjacent control points to be 145 and 35 degrees respectively. These relations are expressed in terms of linear constraints, which effectively restrict the total number of degrees of freedom; complete freedom is only given to the vertical coordinates of the control points located at the leading and trailing edges. Consequently, the parametrization refinement occurs along the spanwise direction, adding more effective design variables. The same restriction on knot interval size still applies; moreover, the added stations are required to satisfy the existing linear constraints.

Figure 7 shows an upward winglet produced during the optimization. The added control points provide additional degrees of freedom to make the winglet more or less normal to the horizontal wing. The last two refinements fail to provide sufficient improvement, so the optimization is terminated with 9 spanwise stations. The drag coefficient is reduced from 0.006730 to 0.005835, and the span efficiency is increased from 0.9656 to 1.1137. This result is close to the performance of the optimized winglet configuration obtained by Hicken and Zingg[37] as they reported a span efficiency of 1.147 using 13 spanwise stations for the upward winglet. This optimization result is compared to the optimal solutions if control points are uniformly distributed. Figure 8 shows that the optimization based on evolutionary parametrization reaches a better optimum with fewer design variables.

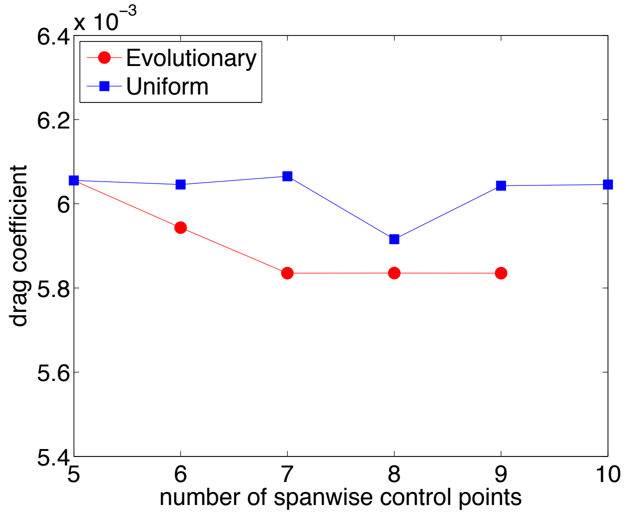

Figure 8. Optimization results comparison

V.E. Box-wing optimization

The evolutionary parametrization is also applied to a box-wing configuration. The initial box-wing geometry has a semi-span of 3.0, a chord length of 1, and NACA0012 sections. The initial height to span ratio is 0.105. It is embedded in a 6-block grid consisting of roughly 6.02×10^5 nodes. The computational grid is approximated using B-spline volumes with 9 control points in the streamwise direction and 5 in the spanwise and vertical directions. The projected area considering the contribution from two horizontal wings is 5.87; it is used as the reference area and constrained to this value during optimization. The initial angle of attack is set to 3.0 degrees and kept fixed. The lift coefficient at this particular angle of attack is 0.1793; it is also constrained to this value.

The control points along the horizontal wings are allowed to move in vertical direction, and the control points on the vertical plate are free to move in the spanwise direction. Again, the control points belonging to one section are coupled to maintain the integrity of the geometry; only the leading and trailing edge control points have complete freedom. In addition, dihedral and anhedral angle limitations are defined between successive control points, so no abrupt bending is allowed. At the junctions of the horizontal wings and the vertical plate, control points are extrapolated based on adjacent sections including the control points at the leading and trailing edges. Besides these linear constraints, a box constraint is imposed to confine the entire geometry within $0 \leq y \leq 3, -0.315 \leq z \leq 0.315$. The parametrization refinements occur along the span and the vertical plate, additional sections are simultaneously inserted at the upper and lower horizontal wings as well as the vertical plate.

Figure 9 shows the geometry deformation at the end of each cycle. The process is terminated because excessive control points have been placed on the vertical plate, i.e. the geometry limitation is reached. The overall performance is depicted in Figure 10. The optimization based on evolutionary parametrization gains substantial benefit from the added design variables, and the drag coefficient is reduced by a considerable amount. However, the optimization results with uniformly placed control points do not exhibit much dependence on the enriched design variables, and the optimization efficiency is clearly lower than the proposed process.

VI. Conclusion

In the present work, a B-spline approximation method is coupled with a knot insertion algorithm to form an evolutionary geometry parametrization algorithm. This algorithm is able to provide gradually increasing design variables for shape optimization problems. An optimization sequence taking advantage of this feature is proposed, continuously selecting critical design variables to improve the design objective. Several aerodynamic shape optimization problems are solved using this proposed process, and the results are compared with optimizations conducted with uniformly refinement parametrizations. These comparisons consistently

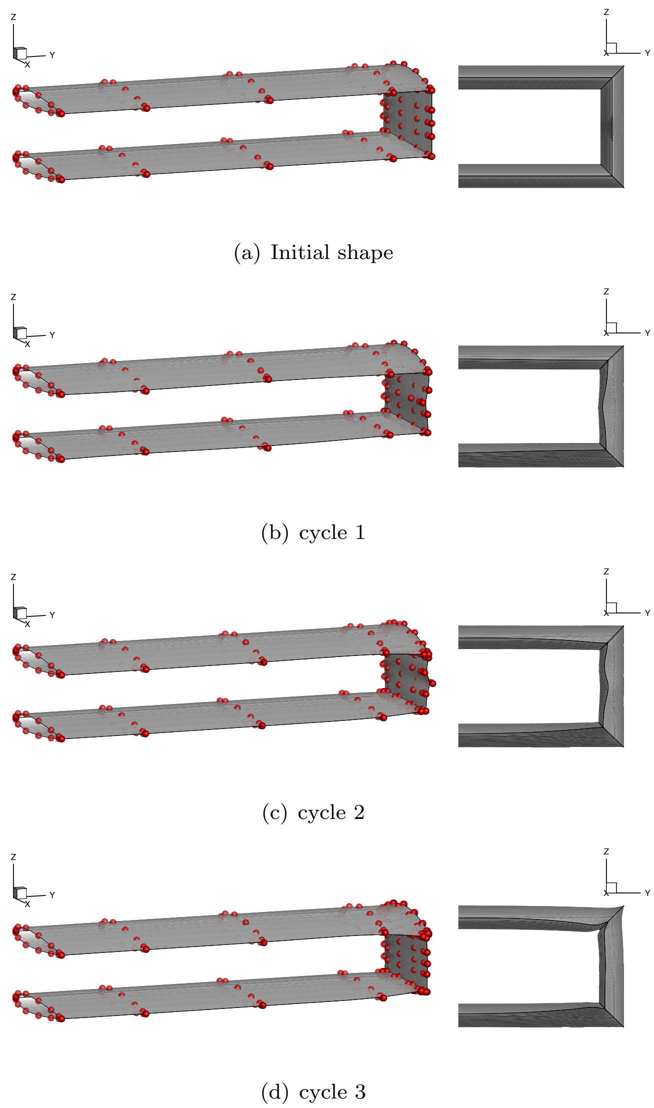

(a) Initial shape

(b) cycle 1

(c) cycle 2

(d) cycle 3

Figure 9. Box-wing optimization

demonstrate that the optimization based on the evolutionary parametrization is more efficient in achieving a better design with fewer design variables. The current process is not fully automated since the implementation of parametrization refinements and the termination conditions still requires experimentation and turning, so future investigation is necessary to improve the automation. Also, evolutionary parametrization is not limited to B-spline formulations; other efficient geometry representation techniques can also be considered and tested.

References

[1] Beux, F. and Dervieux, A., "A Hierarchical Approach for Shape Optimization," *Engineering Computations*, Vol. 11, No. 6, 1994, pp. 25–38.

[2] Andreoli, M., Janka, A., and Desideri, J., "Free-form-deformation Parameterization for Multilevel 3D Shape Optimization in Aerodynamics," Tech. Rep. 5019, INRIA, 2003.

[3] Martinelli, M. and Beux, F., "Multi-level Gradient-based Methods and Parametrization in Aerodynamic Shape Design," *European Journal of Computational Mechanics*, Vol. 17, No. 1-2, 2008, pp. 169–197.

[4] Samareh, J., "Survey of Shape Parameterization Techniques for High-Fidelity Multidisciplinary Shape Optimization," *AIAA J.*, Vol. 39, No. 5, 2001, pp. 877–884.

[5] Castonguay, P. and Nadarajah, S., "Effect of Shape Parameterization on Aerodynamic Shape Optimization," *AIAA-2007-0059, 45th AIAA Aerospace Sciences Meeting and Exhibit*, Reno, Nevada, 8C11 January 2007.

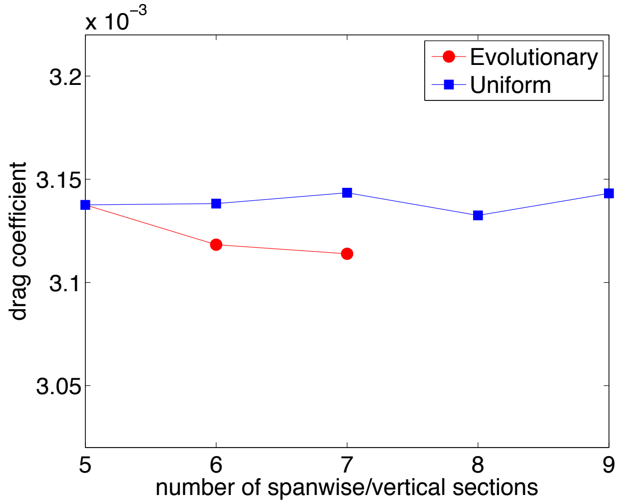

Figure 10. C_D vs. number of sections

[6]Nadarajah, S., Castonguay, P., and Mousavi, A., "Survey of Shape Parameterization Techniques and its Effect on Three Dimensional Aerodynamic Shape Optimization," *AIAA-2007-3837, 18th AIAA Computational Fluid Dynamics Conference*, Miami, FL, 25-28 June 2007.

[7]Jones, R. T., *Wing Theory*, Princeton University Press, 1990.

[8]Oyama, A., Obayashi, S., Nakahashi, K., and Hirose, N., "Aerodynamic Wing Optimization via Evolutionary Algorithms Based on Structured Coding," *Computional Fluid Dynamics Journal*, Vol. 8, No. 4, 2000, pp. 570–577.

[9]Mohammadi, B., "A New Optimal Shape Design Procedure for Inviscid and Visous Turbulent flows," *International Journal for Numerical Methods in Fluids*, Vol. 25, 1997, pp. 183–203.

[10]Morris, A., Allen, C., and Rendall, T., "High-fidelity Aerodynamic Shape Optimization of Modern Transport Wing using Efficient Hierarchical Parameterization," *Int. J. Numer. Meth. Fluids*, Vol. 63, 2010, pp. 297–312.

[11]Song, W. and Keane, A., "A Study of Shape Parameterization Methods for Airfoil Optimisation," *AIAA 2004-4482, 10th AIAA/ISSMO Multidisciplinary Analysis and Optimisation Conference*, Albany, New York, 30 August - 1 September 2004.

[12]Robinson, G. and Keane, A., "Concise Orthogonal Representation of Supercritical Airfoils," *Journal of Aircraft*, Vol. 38, No. 3, 2001, pp. 580–583.

[13]Braibant, V. and Fleury, C., "Shape Optimal Design Using B-Splines," *Computer Methods in Applied Mechanics and Engineering*, Vol. 44, No. 3, 1984, pp. 247–267.

[14]Desideri, J., "Hierarchical Optimum-shape Algorithms using Embedded Bezier Parameterizations," *Numerical Methods for Scientific Computing, Variational Problems and Applications*, 2003.

[15]Duvigneau, R., Chaigne, B., and Desideri, J., "Multilevel Parameterization for Shape Optimization in Aerodynamics and Electromagnetics using a Particle Swarm Optimization Algorithm," Tech. Rep. 6003, INRIA, 2006.

[16]Nemec, M. and Zingg, D. W., "Newton-Krylov Algorithm for Aerodynamic Design using the Navier-Stokes Equations," *AIAA J.*, Vol. 40, 2002, pp. 1146–1154.

[17]Hicken, J. and Zingg, D. W., "Aerodynamic Optimization Algorithm with Integrated Geometry Parameterization and Mesh Movement," *AIAA J.*, Vol. 48, 2010, pp. 401–413.

[18]Kulfan, M., "Universal Parametric Geometry Representation Method," *Journal of Aircraft*, Vol. 45, No. 1, 2008, pp. 142–158.

[19]Farin, G., *Curves and Surfaces for Computer Aided Geometric Design - A Practical Guide*, Academic Press, Boston, 1990.

[20]Tang, Z. and Desideri, J., "Towards Self-adaptive Parameterization of Bezier Curves for Airfoil Aerodynamic Design," Tech. Rep. 4572, IRNIA, 2002.

[21]Hoschek, J. and Lasser, D., *Fundamentals of Computer Aided Geometric Design*, A. K. Peters, Ltd., Natick, MA, USA, 1993, Translator-Schumaker, Larry L.

[22]de Boor, C., *A Practical Guide to Splines*, Springer-Verlag Berlin and Heidelberg GmbH & Co. K, December 1978.

[23]Hoschek, J., "Intrinsic Parametrization for Approximation," *Comput. Aided Geom. Des.*, Vol. 5, No. 1, 1988, pp. 27–31.

[24]Boehm, W., "Inserting New Knots into B-spline Curves," *Computer-Aided Design*, Vol. 12, 1980, pp. 199–201.

[25]Piegl, L., "Modifying the Shape of Rational B-splines. Part 1: Curves," *Computer-Aided Design*, Vol. 21, No. 8, Oct. 1989, pp. 509–518.

[26]Nemec, M., Zingg, D. W., and Pulliam, T. H., "Multipoint and Multi-Objective Aerodynamic Shape Optimization," *AIAA J.*, Vol. 42, 2004, pp. 1057–1065.

[27]Truong, A., Oldfield, C., and Zingg, D. W., "Mesh Movement for a Discrete-Adjoint Newton-Krylov Algorithm for Aerodynamic Optimization," *AIAA J.*, Vol. 46, 2008, pp. 1695–1704.

[28]Hicken, J. and Zingg, D. W., "A Parallel Newton-Krylov Solver for the Euler Equations Discretized Using Simultaneous Approximation Terms," *AIAA J.*, Vol. 46, 2008, pp. 2773–2786.

[29]Hicken, J. and Zingg, D., "Globalization Strategies for Inexact-Newton Solvers," *AIAA 2009-4139, 19th AIAA Computational Fluid Dynamics*, San Antonio, Texas, 22 - 25 June 2009.

[30]Gill, P., Murray, W., and Saunders, M., "SNOPT: An SQP Algorithm for Large-Scale Constrained Optimization," *SIAM Journal on Optimization*, Vol. 12, 2002, pp. 979–1006.

[31]Jameson, A., "Aerodynamic Design via Control Theory," *J. Sci. Comput.*, Vol. 3, No. 3, 1988, pp. 233–260.

[32]Sherar, P., Thompson, C., Xu, B., and Zhong, B., "An Optimization Method based on B-spline Shape Functions & the Knot Insertion Algorithm," *World Congress on Engineering*, 2007, pp. 862–866.

[33]Duvigneau, R., "Adaptive Parameterization using Free-form Deformation for Aerodynamic Shape Optimization," Tech. Rep. 5949, INRIA, 2006.

[34]Zingg, D. W., Nemec, M., and Pulliam, T. H., "A Comparative Evaluation of Genetic and Gradient-Based Algorithms Applied to Aerodynamic Optimization," *REMN*, Vol. 17, 2008, pp. 103–126.

[35]Zingg, D. and Billing, L., "Toward Practical Aerodynamic Design through Numerical Optimization," *AIAA 2007-3950, 18th AIAA Computational Fluid Dynamics Conference*, Miami, FL, June 2007.

[36]Anderson, J. D., *Foundamentals of Aerodynamics*, McGraw-Hill, 2001.

[37]Hicken, J. E. and Zingg, D. W., "Induced-Drag Minimization of Nonplanar Geometries Based on the Euler Equations," *AIAA J.*, Vol. 48, No. 11, 2010, pp. 2564–2575.

[38]Kroo, I., "Drag Due to Lift: Concepts for Prediction and Reduction," *Annual Review of Fluid Mechanics*, Vol. 33, No. 1, 2001, pp. 587–617.